Structural Variations as a Function of Surface Adsorption in Nanostructured Particles

T. Belin, N. Millot,* F. Villiéras, O. Bertrand, and J. P. Bellat

L.R.R.S.-U.M.R. 5613/C.N.R.S., Université de Bourgogne, 9 Avenue Alain Savary, B.P. 47870, 21078 Dijon Cedex, France

Received: September 23, 2003; In Final Form: December 29, 2003

Macroscopic (adsorption isotherm and micro-calorimetry measurement) and microscopic (in situ X-ray diffraction and IR spectroscopy) approaches were used to study the influence of water adsorption on γ-Fe_2O_3 nanoparticles. A nonmonotonic variation of γ-Fe_2O_3 lattice parameter is revealed when the relative water pressure (p/p_0) increases from 0.03 to 0.96 with a maximum deviation for $p/p_0 \approx 0.1$. With IR spectroscopy, similar results were observed since a modification of γ-Fe_2O_3 structural bands has been shown. In situ investigations as well as thermodynamics considerations lead to one important conclusion: the variation of the lattice parameter is in relation with the strains induced during the formation of water monolayer on the nanoparticles surface.

1. Introduction

The physical and chemical properties of nanosized materials exhibit substantial differences from those of micrometric materials. The intrinsic properties are strongly influenced by the surface (via the surface energy) at the nanometric scale. For instance, the Laplace law, used as the main relationship between lattice parameter and crystallite size, takes care of both surface energy and grain size influence. Nevertheless, the original Laplace law implies that the internal pressure in the crystallite is more important in fine crystallites than in coarse ones. Therefore, a lattice parameter decrease would be observed when crystallite size decreases. Since the opposite is observed,[1,2] a derived Laplace law that introduce surface stress instead of surface energy has been developed by Perriat to take care of $BaTiO_3$ properties in fine powders.[3,4] Nevertheless, the surface stress necessary to explain the experimental lattice parameter variation is prohibitive (>10 J·m^{-2}): it is then necessary to take into account the chemical control of the material and especially solid/adsorbed compounds interfacial energy, which means the adsorption state of the solid. In the case of $BaTiO_3$,[2] it is the lack of control of the amount of hydroxide in these powders treated at different temperatures that can explain the lattice parameter variation observed with grain size.[5] According to Tsunekawa et al.,[6] it would be the increase in ionicity of Ti ions that can explain the anomalous lattice expansion measured in $BaTiO_3$ single nanoparticles. In both cases, this is in contrast to a decrease often observed in the lattice constant of metal nanoparticles with a decrease of particle size.[7] In this latter study, the authors found that there is a tendency for the distance between the first and the second layers to contract 2.5−4.5%. In conclusion, the surface has an influence on the lattice parameter and especially for the first atomic layers, which is the reason the aim of this study is to show the water adsorption influence on the structure of nanometric particles.

Iron oxides, key material in several important processes (magnetic and catalytic properties[8]), have been chosen for this new study. Maghemite γ-Fe_2O_3, the ferrimagnetic cubic form of Fe(III) oxide, was closely related to the structure of inverse spinel Fe_3O_4 but differs from the latter by the presence of vacancies distributed on the cation sublattice. It has been suggested that the vacancies can be distributed at random (space group $Fd\bar{3}m$) or ordered as the lithium cation in $LiFe_5O_8$ (space group $P4_132$).[9−12] Its formula can be written $(Fe^{3+})[Fe_{5/3}^{3+}\square_{1/3}]O_4$ where ( ) and [ ] designate respectively tetrahedral and octahedral coordination. In these iron oxides, a change of the cation-to-anion ratio in the cubic phase leads to a deviation from oxygen stoichiometry, $Fe_{3(1-\delta)}O_4$. δ is directly related to the fraction of Fe^{2+} that is oxidized into Fe^{3+} and δ_{max} corresponds to the highest valence of each cation ($\delta_{max} = 1/9$ for Fe_2O_3). In room conditions and even in less restricted conditions (temperature lower than 773 K and p_{O_2} higher than 10^{-5} Pa), the Fe^{2+} cations are not thermodynamically stable and are almost completely oxidized to Fe^{3+}, so that nanometric compounds homogeneous in chemical composition with $\delta \cong 0$ cannot be investigated in room conditions.[13] That is why maghemite ($\delta = \delta_{max}$), rather than magnetite ($\delta = 0$), has been chosen for this study. We could also notice that these oxide nanoparticles are used in the nanohybrid research area.[14] So, the comprehension of their surface interactions is really useful for new nanohybrid development. The surface state could be modified by several molecules: a good interaction with surface could be obtained with a polar molecule. Water vapor, which is an essential and all-purpose compound, has been chosen to maintain simplicity in experimental techniques and to obtain a better interaction with the solid surface. Moreover, water molecule interactions with a solid surface (oxide or metal) have been extensively studied.[15−21] For example, it is well-known that γ-Fe_2O_3 surfaces are stabilized by water molecules to reduce their surface dipolar moment.[22,23]

2. Experimental Section

2.1. Synthesis and Characterization of γ-Fe_2O_3 Nanocrystallites. A range of γ-Fe_2O_3 nanoparticles, homogeneous in size and oxygen stoichiometry, has been prepared by soft chemistry, using coprecipitation of cation precursors $FeCl_3 \cdot 6H_2O$ and $FeCl_2 \cdot 4H_2O$ by adding an ammonia solution.[24,25] The solution was then centrifuged and washed to eliminate chloride

* To whom correspondence should be addressed. E-mail: nmillot@u-bourgogne.fr.

10.1021/jp0310899 CCC: $27.50
Published on Web 04/06/2004

impurities. The centrifugation/wash cycle was pursued until "sol" appearance. A freeze-drying process allowed us to collect a highly divided powder. All powders were submitted to a thermal treatment to eliminate remaining impurities and to produce γ-Fe_2O_3 nanoparticles (all remaining Fe^{2+} cations were oxidized in Fe^{3+}). The conditions of the thermal treatment temperature have been determined by the control of four parameters: the elimination of remaining impurities, the oxygen stoichiometry, the crystallites size, and the transformation temperature between γ- and α-Fe_2O_3 forms (it is well-known that γ-Fe_2O_3 is transformed to hematite α-Fe_2O_3 at a temperature between 523 and 873 K as a function of its previous history[26−29]). Samples were inserted at room temperature in a tubular furnace, heated at 2 K·min^{-1} up to 523 K under air atmosphere, and then kept in the furnace for 4 h. Maghemite samples were then cooled rapidly to room temperature.

All powders synthesized by the previous method were characterized by X-ray diffraction. Room temperature XRD patterns were collected on a Siemens D5000 automatic powder diffractometer, operating at 35 mA and 50 kV.[30] Fluorescence effects were minimized by using Cu Kβ radiation and correction for instrumental broadening was determined from a standard reference material, annealed BaF_2. Pseudo-Voigt peak profile analysis, using the Langford method,[31,32] was performed to determine both the average crystallite size (size of a region over which the diffraction is coherent) and crystallographic imperfections (microdistortions, stacking faults, ...). HRTEM was carried out using an HITACHI hnar 9000 microscope operating at 200 kV (Cs = 0.7 nm, nominal resolution 0.18 nm). The HRTEM images were digitized and an analysis performed using the Digital Micrograph package to investigate both the shape and the granulometric distribution of the nanoparticles. Surface area measurements have been performed using AUTOSORB apparatus with N_2 adsorbing gas. Samples (150−200 mg of powder) were outgassed "in situ" at 493 K. The BET method has been used in the calculation of surface area values from the isotherm of nitrogen adsorption. The mean apparent particle diameter of γ-Fe_2O_3 crystallites was inferred from surface area supposing that nanometric crystallites have a smooth and spherical shape with a narrow granulometric distribution. The X-ray photoelectron spectrometry (XPS) was used to determine the hydroxide amount on the surface of oxide by splitting up the oxygen 1s peak (contributions of hydroxide and lattice oxygen). These analyses were carried out with a Ribber Mac2 semi-imaging analyzer using 300-W Al Kα radiation (1486.6 eV). The samples consisted of compacted γ-Fe_2O_3 powder. The oxygen 1s spectrum was decomposed into two components by fitting with Gaussian (90%)−Lorentzian (10%) peaks. In the fitting procedure, fwhm were fixed: 1.7 eV for the 1s O peak and 2.5 eV for the hydroxide groups. The chemical shifts between hydroxide groups and 1s O contributions were chosen to be equal to 1.9 eV.

These characterizations allowed us to check the validity of our thermal treatment to obtain model materials for this study.

2.2. Macroscopic Experimental Investigation of Water Adsorption. Water vapor pressure in an enclosed space was generated by a thermoregulated cold point containing bidistillate water. Obtaining water vapor pressure in the 70−3500 Pa range was allowed by control of this cold point temperature (from 248 to 300 ± 0.5 K). A secondary vacuum was performed thanks to a zeolite pump ($p_{max} = 2.5 \times 10^{-3}$ Pa). The water vapor equilibrium can be described by the Antoine relation to known water vapor pressure generated by liquid water as a function of temperature.

Thermogravimetry under controlled vapor pressure was used to study the adsorption of water vapor.[21,33] The mass of the sample was about 15 mg. Before each experiment, the maghemite was activated "in situ" at 493 K under 1.5×10^{-3} Pa for 15 h. The adsorption−desorption isotherms were drawn step by step using a static method. Once a plateau of mass was recorded, a following equilibrium was reached by varying the pressure. The temperature of adsorption was 298 K and the water pressure ranging from 82 to 3500 Pa.

The adsorption heats of water vapor were determined by differential calorimetry (C80 Setaram calorimeter) coupled with manometry. This technique allowed the simultaneous measurement of both the adsorbed amount and heat of adsorption and has been described in detail already.[34] The sample mass was 650 mg and the activation conditions were the same as for thermogravimetry. The heats of adsorption measured under our experimental conditions were equivalent to differential molar adsorption enthalpies $\Delta_{ads}\dot{H}_m(T)$, which also correspond to isosteric adsorption heats Q_{iso}.

Another experimental device was used to investigate lower relative pressure ranges. Low water vapor pressure adsorption measurements were carried out in a continuous gravimetric apparatus built around a MK2-M5 CI Electronics Ltd symmetric balance. Pressures were measured using Druck $0-10^3$ and $0-10^5$ Pa absolute pressure sensors. The pressure accuracy was 0.02% of the read pressure. Water vapor was supplied from a source kept at 314 K through a Grandville-Philips leak valve at a slow flow rate to ensure quasiequilibrium conditions at all times.[35] The adsorption isotherms, mass adsorbed at 303 K versus quasiequilibrium pressure, were directly recorded by a computer in the 10^{-4} to 3×10^4 Pa range. Sample outgassing was performed directly in the adsorption device for 4 days at 493 K with a secondary vacuum of 1×10^{-5} Pa. The frequency of the pressure recording was adjusted after each measurement to record more than 100 experimental points per unit of $\ln(p/p_0)$. Due to the large number of experimental data points acquired by the quasiequilibrium method, the experimental derivative of the adsorbed quantity as a function of the logarithm of relative pressure can be calculated accurately.[36] Indeed, it is well-known that a derivative of an adsorption isotherm is much more sensitive to the nature of an adsorption system than the isotherm itself. In the low-pressure range, the derivative isotherms correspond to the first layer adsorption free energy distributions and can be regarded as fingerprints of interactions between given solid/probe couples.[36,37]

2.3. Microscopic Experimental Investigation of the Water Adsorption. Both nanometric sizes of particles and "in situ" experimental devices were required to study surface phenomena in relation to structural properties. As the nature of adsorbed compounds on the γ-Fe_2O_3 surface was known by previous characterizations, it was possible to investigate qualitative structure variations and to follow vibrational mode modifications by "in situ" infrared spectroscopy. The device used was a Perkin-Helmer 1725X FTIR spectrophotometer with an "in situ" assembly. Low thickness disks (50 mg and 13 mm diameter) containing pure γ-Fe_2O_3 powders were obtained using a mechanical pressure of 150 kg·cm^{-2}. An activation process (thermal treatment at 493 K under secondary vacuum) was performed to clean the surface of nanoparticles (Figure 1). Relative water pressures were generated as described in the Macroscopic Experimental Section. For each relative water pressure, a spectrum was recorded over 30 min. This allowed us to follow band positions with the increasing amount of adsorbed water.

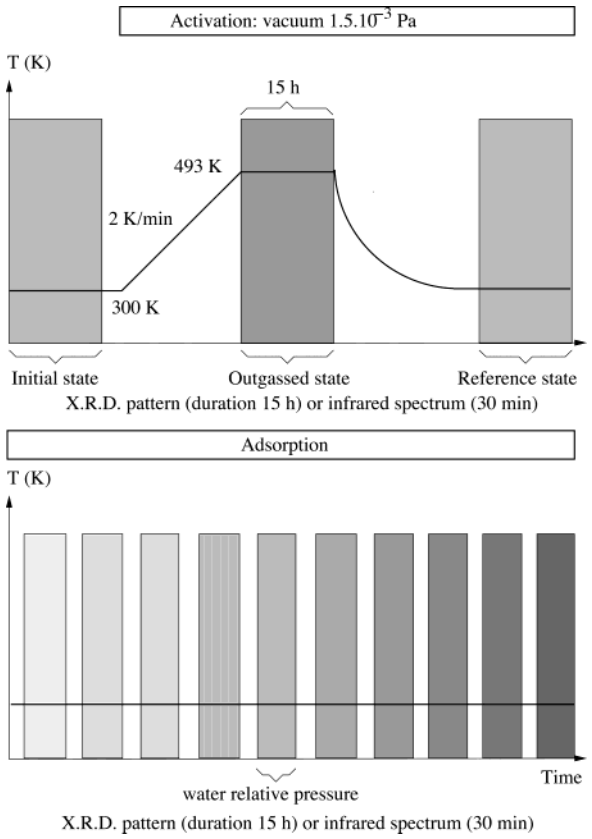

Figure 1. "In situ" protocol used on X-ray and infrared experimental devices. The sample was first outgassed at 493 K for 15 h. Then, this outgassing process was followed by a step-by-step adsorption cycle: relative water pressure was applied to the sample and an equilibrium was reached before measurements.

"In situ" X-ray diffraction experiments were conducted to determine the lattice parameter variations with γ-Fe_2O_3 surface state. XRD patterns were collected using an INEL CPS120 X-ray position sensitive detector and a quartz monochromator.[38] All diffraction patterns were performed with the wavelength of Co Kα_1 (λ = 0,178897 nm). An XRD pattern of γ-Fe_2O_3 sample was collected under air atmosphere at 300 K to verify the sample position. Then, under secondary vacuum and at 493 K (the activation temperature), another XRD pattern was performed to control the lack of hematite α-Fe_2O_3. Finally, an XRD reference pattern at 300 K and under secondary vacuum was used as a reference for data analysis. Adsorption steps of water vapor were performed on the sample under saturated vapor pressure without closing the cold point. A 4-h delay was kept to allow an equilibrium state between the water and the sample system. For each relative water pressure, 15-h XRD patterns were collected (Figure 1). Pattern decomposition was carried out by means of both the profile fitting program PROFILE (available in the PC software DIFFRAC AT supplied by Siemens) and the Rietveld method using the XND 1.22 software[39] to obtain parameters defining the position, the height, the area, the integral width, and the shape of Bragg reflections. The powder lattice parameters were deduced from XRD line positions using a least-squares refinement method with home-built software. This method took into account the effect of a sample gap on line positions according to the relation for cubic form used by Sarrazin et al.[40]

3. Results and Discussion

Thanks to synthesis described elsewhere,[25] γ-Fe_2O_3 maghemite particles are obtained after a precipitation stage followed by a thermal annealing at 523 K in nanometric size (9 to 14 nm). They are monocrystalline and without porosity (Table 1).

TABLE 1: Bulk and Surface Properties of Nanometric γ-Fe_2O_3 Powders Obtained after an Annealing at 523 K[a]

	temperature of precipitation (K) =			
	298	323	343	363
BET surface area ($\pm$1 $m^2 \cdot g^{-1}$)	133	116	108	89
BET particle diameter ($\pm$0.2 nm)	9.3	10.6	11.4	13.8
lattice parameter ($\pm$0.0001 nm)	0.8347	0.8349	0.8347	0.8346
δ (see introduction) (maghemite δ = 0.11)	0.106	0.103	0.106	0.106
XRD particle diameter ($\pm$1.0 nm)	8.4	9.2	10.7	12.3

[a] Surface area is obtained by N_2 coverage measurements and used to determine particle diameter. Lattice parameters are calculated from the XRD pattern using refinement of line shape position. The grain size mentionned in the text is that obtained by XRD refinements

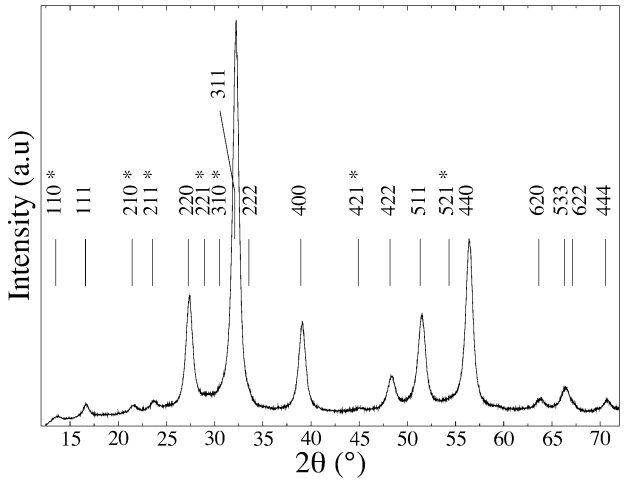

Figure 2. Powder XRD pattern of the maghemite γ-Fe_2O_3 sample (10.7 nm). All peaks are indexed and asterisks illustrate substructure linked to vacancies ordering.

Deviation to the oxygen stoichiometry for each sample is equal to that of maghemite stoichiometry (δ = 0.11). The crystallinity and the purity of these products have already been established.[25]

Figure 2 shows an XRD pattern of the maghemite sample. This pattern could be indexed on the basis of the unit cell corresponding to the $P4_132$ space group, which suggested that the vacancies are perfectly ordered. As proved in ref 25, the grain size effect on the lattice parameter is negligible in the 8−13 nm range. No hematite α-Fe_2O_3 is detected.[25] Morphology of nanoparticles has been investigated with TEM experiments. Low-resolution TEM experiments show a narrow size distribution.[25] To characterize better the powder microstructures, powders have been examined by HRTEM. As observed in Figure 3, crystallites are quite agglomerated and exhibit an hexagonal shape. This particular shape already has been observed in other spinel compounds.[41−43] There is no surrounding boundary of an amorphous nature and HRTEM micrographs demonstrate that there are no structural defects in powders synthesized by soft chemistry in agreement with XRD profile analysis. The crystallite size determined by HRTEM (about 6−8 nm) is the same as the size derived from XRD analysis (8.4 $\pm$ 1.0 nm). As a conclusion for these characterizations, XRD and surface area measurements confirmed the nanometric scale of maghemite nanoparticles synthesized by soft chemistry. Both XRD and TEM experiments showed their very good crystallinity.

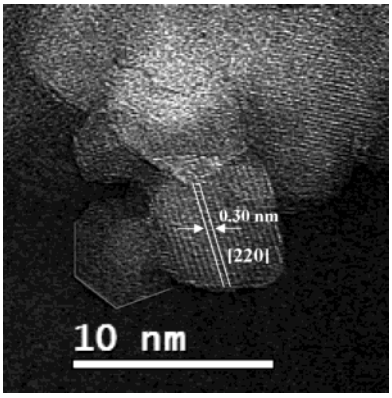

Figure 3. High-resolution image of the nanocrystalline γ-Fe_2O_3 sample precipitated at 298 K and treated at 523 K over 4 h under air atmosphere. The white bars show the 220 lattice fringes, the gray bars illustrate that the particles are faceted.

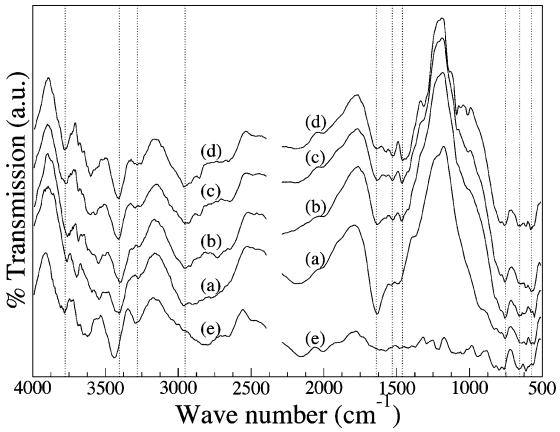

Figure 4. "In situ" infrared spectra obtained from γ-Fe_2O_3 sample (ϕ_{XRD} = 10.7 nm) and used in the determination of activation conditions: (a) sample in air, (b) sample under a secondary vacuum of 2.5×10^{-3} Pa for 2 h, (c) 8 h, and (d) 15 h, and (e) after thermal treatment at 493 K for 15 h. γ-Fe_2O_3 bands are in the range 800−500 cm^{-1}, water physisorbed at 1640 cm^{-1}, and hydroxide bands are in range 4000−3000 cm^{-1}.

The thermal activation conditions have to be well-determined before an attempt is made to study water adsorption on powders. We need to obtain a "clean" surface empty of carbonates or water physisorbed. Moreover, this step should increase the number of adsorption active sites. An infrared study allows us to determine these activation parameters. Nevertheless, infrared spectra remain very difficult to interpret and quantitative measurements also difficult to undertake. Then, the aim of these infrared measurements is only to obtain qualitative information in order to study desorption of compounds adsorbed on the maghemite surface. Infrared absorption bands (at ∼3400, 1640 and in the 800−500 cm^{-1} region) appear in all five spectra obtained under either air or vacuum or after 220 °C thermal treatment (Figure 4). The high-frequency bands (3400 and 1640 cm^{-1}) are assigned to hydroxide and water physisorbed on the maghemite surface. Low-frequency bands (800−500 cm^{-1}) are assigned to the spinel γ-Fe_2O_3 structure. Interpretation of these bands has been proposed by Waldron[44] and White:[45] the ν_1 band (576 cm^{-1}) refers to Fe−O deformation in the octahedral and tetrahedral site while the ν_2 band (420 cm^{-1}) refers only to Fe−O deformation in octahedral sites. These in situ infrared experiments illustrate that the bands around 1640 cm^{-1} are strongly reduced as early as samples are placed under the secondary vacuum. This is linked to the desorption of water physisorbed on the maghemite surface. The maximum of this desorption is obtained after the thermal treatment at 493 K under the secondary vacuum. Furthermore, carbonate groups present on surface powders (1530, 1460 cm^{-1}) slowly disappear under vacuum and are totally removed after the thermal treatment. The persistence of bands in the 4000−3000 cm^{-1} range shows the difficulty in removing hydroxide groups from the surface: only a small portion is removed at a temperature of 493 K under vacuum.[46,47] Increasing the thermal temperature solves this problem but induces an increase of the α-Fe_2O_3 hematite ratio in samples due to the γ-/α-Fe_2O_3 phase transition.[29] We have also noticed the lack of structure band variations. Under a 2.5×10^{-3} Pa secondary vacuum and whatever the time (2, 8, or 15 h), no significant variation of the band positions (524, 576, 653, 755, 788, and 829 cm^{-1}) is detected (maximum shift: 6 cm^{-1}) (Figure 5). However, a general displacement of the band position is shown with the activation thermal treatment but this is due to the temperature effect.

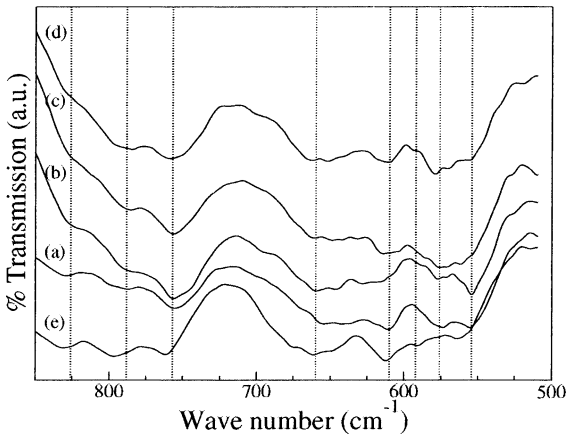

Figure 5. Enlargement of γ-Fe_2O_3 (ϕ_{XRD} = 10.7 nm) infrared spectra (Figure 4) in structure band area: (a) sample in air, (b) sample under a secondary vacuum of 2.5×10^{-3} Pa for 2 h, (c) 8 h, and (d) 15 h, and (e) after thermal treatment at 493 K for 15 h.

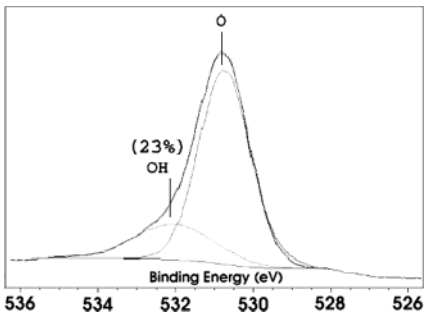

Figure 6. Oxygen 1s decomposition from the X.P.S. spectrum of the γ-Fe_2O_3 sample (ϕ_{XRD} = 10.7 nm). A contribution of hydroxide groups (23%) was revealed. For this decomposition, an energetic gap between the $2p^{3/2}$ Fe peak and the 1s O peak remained constant (180.5 eV). Only the position and width of the hydroxide peak and the width of the oxygen peak are modified.

As we have discussed before, there are a large number of hydroxide groups on the maghemite surface. In literature,[22,23] a stabilization of {111} and {100} γ-Fe_2O_3 surfaces or more accurately a compensation of bipolar moment could be obtained thanks to hydroxide groups. XPS measurements realized on the γ-Fe_2O_3 sample lead to the determination of the experimental amount of hydroxide groups of about 20% of the total contribution of oxygen at the surface of particles (Figure 6).

To identify the different mechanisms in water adsorption on γ-Fe_2O_3 samples, an adsorption isotherm is realized by thermogravimetry (Figure 7). The adsorption/desorption isotherm

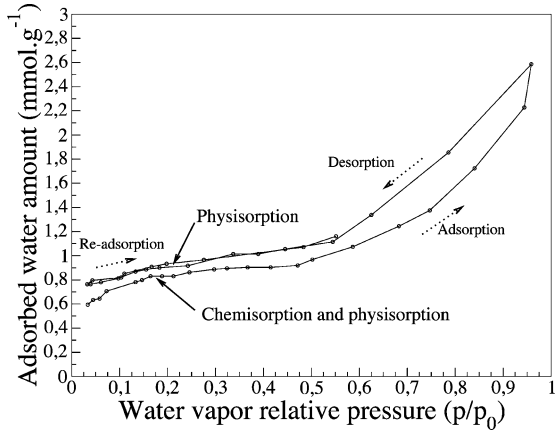

Figure 7. Water adsorption−desorption isotherm obtained by thermogravimetry ($T = 298$ K). The maghemite γ-Fe_2O_3 sample ($\phi_{XRD} = 10.7$ nm) is first outgassed at 493 K for 15 h with a secondary vacuum (1.5×10^{-3} Pa).

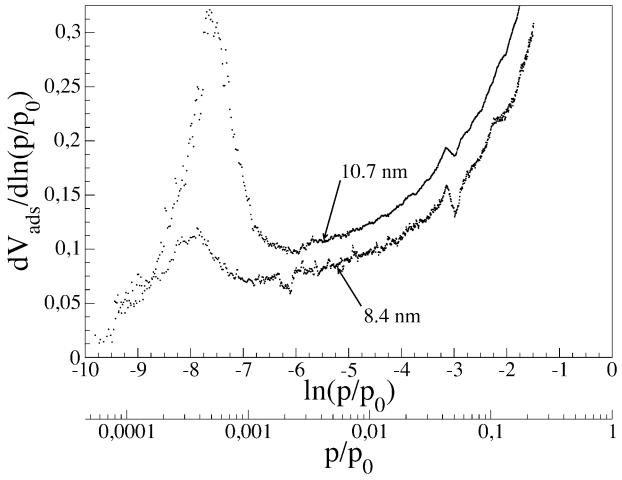

Figure 8. Water adsorption derived isotherm of γ-Fe_2O_3 nanoparticles obtained with low water vapor relative pressure ($T = 303$ K). The sample is first outgassed at 493 K for 4 days with a secondary vacuum (1×10^{-5} Pa).

exhibits, at least, two different stages: (i) an adsorption step combining chemisorption and physisorption (first branch) followed by (ii) a desorption step where physisorption appears to be the only active mechanism (second branch). A readsorption step confirmed these assumptions (third branch). The second branch exhibits a type II shape in the IUPAC classification, characteristic of the adsorption on a nonporous solid.[48] With this technique (a static method), no information is revealed about the amount of adsorbed water at very low relative pressure. This could be realized using isotherms obtained from another experimental device allowing the investigation of this low vapor pressure range. Derived isotherms are calculated to extract important data from the very low relative pressure domain (Figure 8); the main idea is to obtain information about the amount of adsorbed water and, for a second time, to check the formation of the water monolayer. With these derived isotherms, two different areas are detected: a unique peak is revealed at very low relative pressure ($p/p_0 = 4.7 \times 10^{-4}$ for 8.4 nm and 3.2×10^{-4} for 10.7 nm), and for higher relative pressures, the derived isotherms increase regularly. The interpretation of these shapes is relevant of surface energetic heterogeneity. The presence of a unique peak is associated with the existence of only one type of high-energy adsorption sites. To interpret this peak, two different assumptions are used: these sites are filled

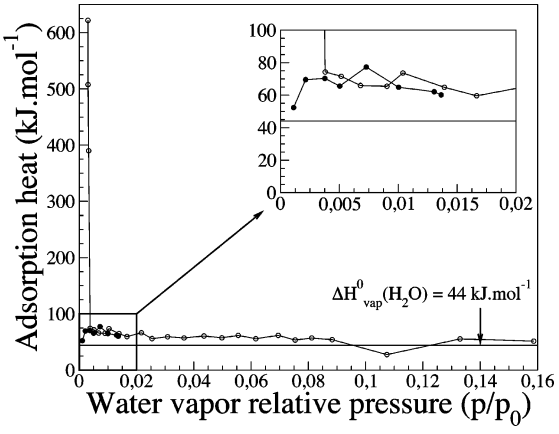

Figure 9. Water adsorption heat as a function of relative pressure obtained from γ-Fe_2O_3 nanoparticles (10.7 nm): sample outgassed at 493 K for 15 h with secondary vacuum (1.5×10^{-3} Pa) (○) and sample without thermal activation (●). With this last sample, only physisorption phenomena were identified in comparison with the activated sample where physisorption and chemisorption were visible.

by water molecules which are either (i) dissociated with the chemisorption step or (ii) strongly structured on nanoparticle surfaces. At higher relative water pressure ($p/p_0 > 0.1$), derived isotherms exhibit a steady increase, which has been linked to the formation of multilayer mechanisms.

Energetic measurements are carried out along the adsorption isotherm. A microcalorimetric study at the first step of adsorption is performed on the 10.7 nm sized γ-Fe_2O_3 sample (Figure 9). With activated powders, heat of adsorption curves as a function of relative pressure show multiple steps (circles on Figure 9). For relative pressure below 0.005, the absolute value of adsorption heat is about 630 kJ·mol^{-1}. This value is characteristic of a water chemisorption on high-energy adsorption sites[49] that are released during the activation step. This measurement indicates a possible partial re-hydroxylation of the oxide surface. For relative pressures higher than 0.005 and lower than 0.1, adsorption heat is within 75−50 kJ·mol^{-1}; this result is characteristic of the formation of a water monolayer onto the γ-Fe_2O_3 surface. Indeed, the adsorption heat obtained is higher than that of water vaporization heat (44 kJ.mol^{-1}) and is evidence of the interactions which take place between the adsorbed water molecules and the oxide surface. When the relative pressure is higher than 0.1, adsorption heats become weaker and could be compared to the water vaporization heat. This value is characteristic of molecular interaction between molecules in water multilayers.[21] Same calorimetric measurements are led on nonactivated powders (black dots in Figure 9 inset). Only one value for adsorption heat is detected (∼60 kJ·mol^{-1}). This value is similar to water vaporization heat (44 kJ.mol^{-1}). This verification proves that, after activation, water is chemisorbed on the surface of particles at low relative pressure. So, in this low pressure range, water chemisorption is the main process in comparison with water structuring. At this stage, adsorption isotherms (Figures 7 and 8) as well as thermodynamic considerations (Figure 9) have helped to depict a possible scenario; indeed, simultaneous with the end of the water chemisorption step and at a relative pressure lower than 0.1, water clusters (round to Fe−OH site) or water physisorbed monolayer are formed. Then, water multilayers take over at a relative water pressure above 0.1.

A microscopic approach is needed to study water adsorption effects on the structure of γ-Fe_2O_3. As stated previously, two experimental devices are used: "in situ" infrared spectroscopy and "in situ" X-ray diffraction. In all cases, samples are

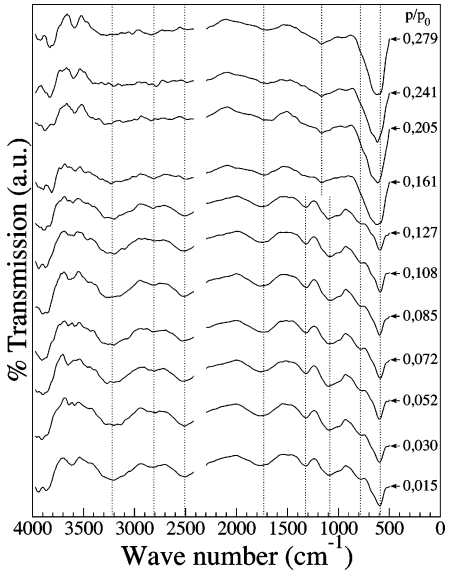

Figure 10. "In situ" infrared spectra of the γ-Fe_2O_3 sample (8.4 nm) obtained as a function of relative water pressure ($T = 298$ K). Main bands were marked with dotted lines. The number of curves was reduced to make the figure more clear.

submitted to activation thermal treatment, and then measurements are realized under increasing relative water pressure. The infrared spectra obtained are shown in Figure 10. Major bands are those of hydroxide groups (4000−3000 cm^{-1}), water (1760 cm^{-1}), and the maghemite structure (580 cm^{-1}). These groups of bands already have been detailed accurately, nevertheless some discrepancies exist and could be due both to the difference of the sample grain size (8.4 nm instead of 10.7 nm) or most probably to the experimental conditions which are different: desorption in the case of Figure 4 instead of the first steps of adsorption in the case of Figure 10. In the literature, several types of interaction have been described: Bands at 3200 and 2800 cm^{-1} are characteristic of hydroxide groups. A second series is attributed to liquid water in interaction with a surface: 1700, 1327, and 1090 cm^{-1}.[50] A third band at 2510 cm^{-1} is induced by water dissociation phenomena or water−water interaction on the maghemite surface: this band is typical of strong hydrogen bonds.[51] The last series is linked to the γ-Fe_2O_3 band (800 and 580 cm^{-1}).[46,52] When relative water pressure increases up to 0.127, there is no modification of infrared spectra shape. Only a strong interaction of water with the maghemite surface is revealed by the experimental shift of the second band series (from 1700 to 1760 cm^{-1}). But between 0.127 and 0.161 cm^{-1}, two absorption bands (1090 and 1327 cm^{-1}) merged into one band at 1153 cm^{-1}. This is related to a strong variation of water/surface interactions. To give a better interpretation of these phenomena, the displacement of major bands during the water adsorption isotherm is shown Figure 11. Infrared band positions are greatly displaced above a relative pressure of 0.125. Maximal variation was about 7% and γ-Fe_2O_3 structural bands and water bands are submitted to the most important displacement. On the contrary, hydroxide groups are not influenced by the increase of relative water pressure. Therefore, there is a relation between physisorbed water and γ-Fe_2O_3 structure: the most significant variations are observed above a relative pressure of about 0.125 while adsorption sites for water dissociation are already filled. This "critical" relative pressure rather corresponds to the end of the water monolayer formation.

X-ray diffraction is a statistical method that allows us to follow "in situ" the structural evolutions of nanometric powders. As clearly reported on Figure 12, the γ-Fe_2O_3 lattice parameter

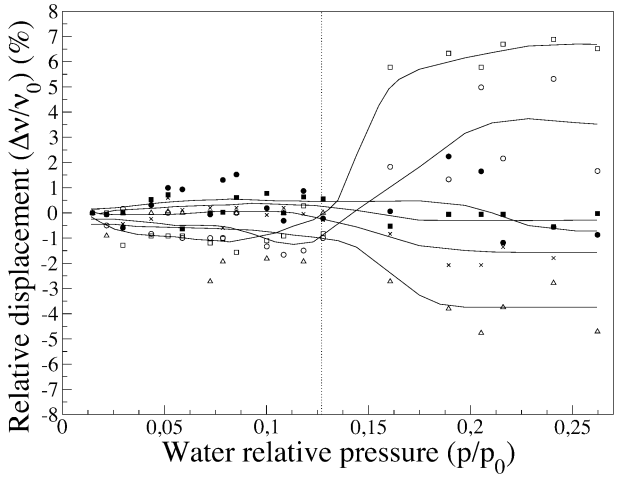

Figure 11. Relative displacement ($\Delta\nu/\nu_0$) of infrared adsorption bands as a function of relative water pressure obtained on γ-Fe_2O_3 nanoparticles. Lines were drawn only as guides for the eye: maghemite structure (○, □) 800, 500 cm^{-1}; water (△) 1700 cm^{-1}; hydrogen bonds (×) 2500 cm^{-1}; hydroxide groups (●, ■) 3200, 2800 cm^{-1}.

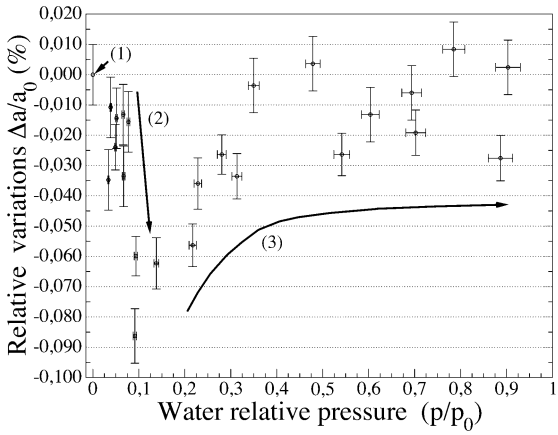

Figure 12. Relative variations $\Delta a/a_0$ of the γ-Fe_2O_3 lattice parameter (sample with a mean grain size of 10.7 nm) as a function of relative water pressure and obtained from "in situ" XRD patterns: (1) lattice parameter after the activation thermal treatment at 493 K for 15 h and under a secondary vacuum of 1.5×10^{-3} Pa; (2) decrease of lattice parameter for relative pressure under 0.1; and (3) increase of lattice parameter up to the recovery of the room conditions value.

depends strongly on the relative water pressure. When samples are placed under an increasing relative water pressure, two steps are observed: at a relative pressure below 0.1, the lattice parameter drops perceptibly and rapidly (−0.087% compared with the value obtained after the activation treatment 0.8345-(8) nm) to reach a minimum value equal to 0.8338(5) nm for a relative pressure of about 0.1. Above this value, the lattice parameter steadily increases to reach the plateaulike domain for room conditions (0.8346(0) nm). Thus, the two domains depicted in Figure 12 force us to consider a nonmonotonic behavior of the γ-Fe_2O_3 lattice parameter versus relative water pressure. This peculiar behavior is difficult to interpret; nevertheless, some hypothesis may be considered at this stage, like complex interactions between various parameters. On the contrary, no microdistortion evolutions are involved in the process since the XRD line profile investigations during the adsorption steps has not revealed anything (microdistortions estimated to 2.343×10^{-3} for $p/p_0 = 0.15$ and 2.344×10^{-3} for $p/p_0 = 0.279$).

Microcalorimetry experiments have shown that the pressure range for water chemisorption on γ-Fe_2O_3 is below 0.005. As a consequence, structural changes observed by both IR spec-

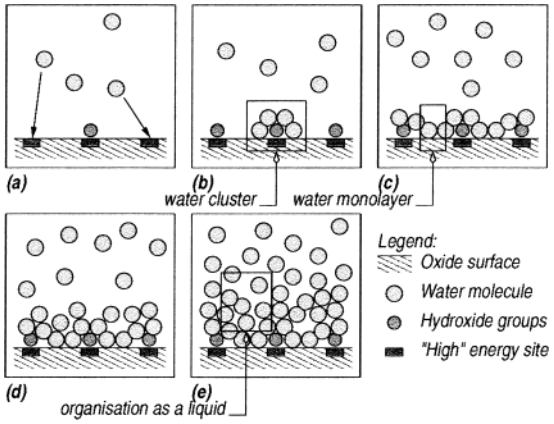

Figure 13. Schematic hypothesis proposed as an explanation of γ-Fe_2O_3 lattice parameter variations with the increase of relative water pressure. (a) At very low water vapor pressure ($p/p_0 < 0.005$), water molecules are dissociated on "high" energy sites. With relative water pressure between 0.005 and 0.1 (b and c), we have noticed a decrease of lattice parameter (XRD) and no influence of water amount on γ-Fe_2O_3 infrared structural bands (FTIR). This step was attributed to the formation of a water monolayer. As a consequence, surface energy and surface stress of nanoparticles are modified. At a relative water pressure above 0.1 (d and e), the return of the lattice parameter to the room conditions value (XRD) and displacement of γ-Fe_2O_3 structural bands (FTIR) have been detected. Here, a multilayer was formed by water molecules and surface stress was modified again due to the presence of additional water molecules and new water organization.

troscopy and XRD could not been explained by chemisorption phenomena. Relative pressures are really different (0.005 as opposed to 0.1 for the maximum of lattice decrease): above a relative pressure of 0.005, maghemite surfaces are only submitted to physisorption phenomena. One of the most convincing explanations for these structural modifications (lattice parameter variations and displacement of vibrational bands) is given by the comparison of all the results described above. Figure 13 illustrates the different adsorption steps. At the end of filling the "high"-energy adsorption sites by water molecules (main dissociative chemisorption step), the increase of relative water pressure leads to the formation of a water monolayer on the γ-Fe_2O_3 surface[53] (Figure 13a). During this step, water molecules are not adsorbed randomly but according to energetic site distribution. In that case, two evolutions are possible: (i) formation of a water cluster from hydroxide groups fixed on the γ-Fe_2O_3 surface and then filling up the water monolayer (Figure 13b) and (ii) regular filling of the water monolayer (Figure 13c). Data extracted from "in situ" experiments do not allow us to make any conclusions about one or the other phenomenon. However, modification of the γ-Fe_2O_3 surface state should involve a modification of the surface strain. The latter played a key role in surface stabilization or surface reconstruction.[54,55] Most of the time, the water molecule structure in the monolayer is similar to bidimensional solid organization. Therefore, the water monolayer contributes to the increase of compression strain on γ-Fe_2O_3, which leads to the observed decrease of the lattice parameter. Strong water structuration on the nanoparticle surface is probably one parameter to take into account. At a relative water pressure above 0.1, water adsorption on the surface induces the formation of water multilayers. The organization of those multilayers is not clear but liquidlike structure may be considered. That is the reason surface interactions decrease to become essentially intermolecular. Consequently, the surface strains are reduced; this relaxation leads to the increase of the lattice parameter observed by "in situ" XRD (see Figure 13d,e). Using Hooke's

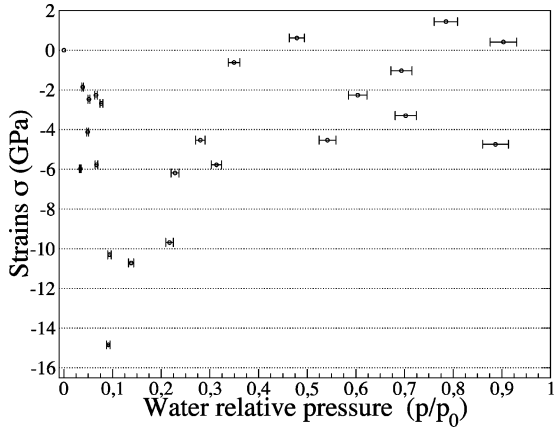

Figure 14. Estimation of strains in γ-Fe_2O_3 oxide nanoparticles as a function of relative water pressure. Data were valid in the elastic range and were calculated from lattice deformations with an estimated Young modulus in oxide nanoparticles ($E = 3 \times 10^5$ MPa.[56]).

law and assumptions of isotropic strains, strains have been estimated. These data are shown in Figure 14 and are calculated thanks to XRD reflections (220), (311), (400), (422), (511), and (422). The effect of water adsorption on the maghemite structure induces a nonmonotonic strain variation, which is similar to lattice parameter variations. These strains estimated on γ-Fe_2O_3 are only compressive with a maximum at a relative water pressure of about 0.1 ($\sigma_{max} = -14.8$ GPa). In the literature, similar values of strains have been calculated with iron oxide nanoparticles at the time of oxidation experiments.[56] Above a relative pressure of 0.1, a relaxation of strains is observed until the restoration of the initial value.

4. Conclusions

Model γ-Fe_2O_3 nanoparticles have been synthesized by a soft chemistry route using precipitation of Fe(II) and Fe(III) chloride salts in stoichiometric proportions. These powders were characterized with several methods (XRD, TEM, XPS, BET, IR). The use of "in situ" infrared spectroscopy allowed the determination of the thermal activation conditions to eliminate water physisorbed and a maximum number of hydroxyl groups on the surface without modification of oxygen stoichiometry and vacancy distributions. This technique also allowed us to detect structural variations of γ-Fe_2O_3 with the increase of relative water pressure. A "critical" point was brought to the fore at a relative pressure of about 0.127. A complex relation between the γ-Fe_2O_3 structure and water adsorbed on the surface has been demonstrated. It was illustrated by the nonmonotonic lattice parameter variation of γ-Fe_2O_3 nanoparticles during water adsorption. Two different steps were observed: The first was a lattice parameter decrease (0.087%) at low relative pressure. This decrease could be explained by the formation of water monolayer at the surface of nanoparticles. The second step was a lattice parameter increase at high relative pressure, which could be due to the formation of a water multilayer. These two steps were not linked to the chemisorption step as revealed by the microcalorimetric method: indeed, the water chemisorbed range (630 kJ·mol^{-1}) was not studied by "in situ" XRD experiments. Over a 0.005 relative pressure, the heat of adsorption was representative of water physisorption on oxide (50 kJ·mol^{-1}). These structural variations seen both by XRD and IR experiments were due to surface strains brought by the physisorbed water. The water monolayer formed contributed to the increase of compression strain on γ-Fe_2O_3. Then, a relaxation of surface strains occurred when water organization led to water multilayers.

A theoretical approach is needed to complete the understanding of the relation between surface and structure in nanomaterials. Such experiments on iron/oxide core/shell are currently being carried out and are not yet published. The same nonmonotonic structural evolutions are also observed for these materials.

Acknowledgment. The authors would like to thanks Dr. K. Amilain-Basset and Dr. O. Heintz (L.R.R.S., Dijon, France) for their help in X.P.S. measurements and Dr. E. Gautier (I.M.N., Nantes, France) for M.E.T. experiments. Thanks also are extended to Dr. Ch. Valot (L.R.R.S., Dijon, France), Dr. N. Floquet (C.R.M.C2, Marseille, France), and Pr. H. Van Damme (E.S.P.C.I., Paris, France) for helpful discussions.

References and Notes

(1) Ayyub, P.; Multani, M.; Barma, M. *J. Phys. C: Solid State* **1988**, *21*, 2229.
(2) Bernaben, N.; Leriche, A.; Thierry, B. *Fourth Euro Ceramics* **1995**, *5*, 203.
(3) Perriat, P. *Nanostruct. Mater.* **1995**, *6*, 791.
(4) Perriat, P.; Niepce, J. C. *J. High Temp. Chem. Processes* **1994**, *3*, 585.
(5) Perrot-Sipple, F. Ph.D Thesis, University of Burgundy, 1999.
(6) Tsunekawa, S.; Ishikawa, K.; Li, Z. Q.; Kawazoe, Y.; Kasuya, A. *Phys. Rev. Lett.* **2000**, *85*, 3440.
(7) Hansen, L. B.; Stolze, P.; Norskov, J. K. *Phys. Rev. Lett.* **1990**, *64*, 3155.
(8) Dormann, J. L.; Fiorani, D.; Tronc, E. *Adv. Chem. Phys.* **1997**, *98*, 283.
(9) Morales, M. P.; Pecharroman, C.; Gonzalez-Carreno, T. *J. Solid State Chem.* **1998**, *108*, 158.
(10) Morales, M. P.; Andres-Verges, M.; Veintemillas-Verdaguer, S. *J. Magn. Magn. Mater.* **1999**, *203*, 146.
(11) Greaves, C. *J. Solid State Chem.* **1983**, *49*, 325.
(12) Shmakov, A. N.; Kryukova, G. N.; Tsybulya, S. V. *J. Appl. Crystallogr.* **1995**, *28*, 141.
(13) Guigue-Millot, N.; Champion, Y.; Hÿtch, M. J.; Bernard, F.; Bégin-Colin, S.; Perriat, P. *J. Phys. Chem. B* **2001**, *105*, 7125.
(14) Kwon, C. W.; Poquet, A.; Mornet, S.; Campet, G.; Portier, J.; Choy J. H. *Electrochem. Commun.* **2002**, *4*, 197.
(15) Hendewerk, M.; Salmeron, M.; Sommorjai, G. A. *Surf. Sci.* **1986**, *172*, 544.
(16) Whitten, J. L.; Yang. H. *Surf. Sci. Rep.* **1996**, *24*, 55.
(17) Ferry, D.; Glebov, A.; Senz, V. *Surf. Sci.* **1997**, *377*−*379*, 634.
(18) Ismail, H. M.; Cadenhead, D. A.; Zaki, M. I. *J. Colloid Interface Sci.* **1996**, *183*, 320.
(19) Liu, P.; Kendelewicz, T.; Brown, G. E. *Surf. Sci.* **1998**, *417*, 53.
(20) Henderson, M. A.; Joyce, S. A.; Rustad, J. R. *Surf. Sci.* **1998**, *417*, 66.
(21) Moise, J. C.; Bellat, J. P.; Methivier, A. *Microporous Mesoporous Mater.* **2001**, *43*, 91.
(22) Tasker, P. W. *J. Phys. C: Solid State* **1979**, *12*, 4977.
(23) Tamura, H.; Mita, K.; Tanaka, A.; Ito, M. *J. Colloid Interface Sci.* **2001**, *243*, 202.
(24) Millot, N.; Bégin-Colin, S.; Perriat, P. *J. Solid State Chem.* **1998**, *139*, 66.
(25) Belin, T.; Guigue-Millot, N.; Caillot, T.; Aymes, D.; Niepce, J. C. *J. Solid State Chem.* **2002**, *163*, 459.
(26) Cousin, P.; Ross, P. A. *Mater. Sci. Eng.* **1990**, *A130*, 119.
(27) Herrero, E.; Cabanas, M. V.; Vallet-Regi, M. *Solid State Ionics* **1997**, *101*−*103*, 213.
(28) Ennas, G.; Marongiu, G.; Musinu, A. *J. Mater. Res.* **1999**, *14*, 1570.
(29) Millot, N.; Belin, T.; Bovet, N.; Gailhanou, M. *J. Appl. Crystallogr.* To be submitted for publication.
(30) Oetzel, M.; Heger, G. *J. Appl. Crystallogr.* **1999**, *32*, 799.
(31) Halder, N. C.; Wagner, C. N. J. *Acta Crystallogr.* **1966**, *20*, 91.
(32) Langford, J. I. *NIST Spec. Publ.*: *Acc. Powder Diff.* **1992**, 110.
(33) Simonot-Grange, M. H. *Clay Miner.* **1979**, *27*, 423.
(34) Simonot-Grange, M. H.; Bertrand, O.; Pilverdier, E.; Bellat, J. P.; Paulin, C. *J. Therm. Anal.* **1997**, *48*, 741.
(35) Poirier, J. E.; François, M.; Cases J. M.; Rouquerol J. *Proceedings of the second engineering foundation conference on fundamental adsorption*; Liapis A. I., Ed.; AIChE Pub.: New York, 1987; pp 473−482.
(36) Villiéras, F.; Cases, J. M.; François, M.; Michot, L.; Thomas, F. *Langmuir* **1992**, *8*, 1789.
(37) Villiéras, F.; Michot, L. J.; Bardot, F.; Chamerois, M.; Eypert-Blaison, C.; François, M. G.; Gérard, G.; Cases, J. M. *Surf. Heter. Min., C. R. Geosci.* **2002**, *334*, 597−609.
(38) Deniard, P.; Evain, M.; Barbet, J. M. *Mater. Sci. Forum* **1991**, *79*−*82*, 363.
(39) Berar, J. F.; Baldinozzi, G. *IUCR-CPD Newslett.* **1998**, *20*, 3.
(40) Bernard, F.; Charlot, F.; Sarrazin, P. *J. Phys. IV* **1996**, *6*, 103.
(41) Gillot, B.; Rousset, A.; Chassagneux, F. *J. Solid State Chem.* **1988,** *76*, 355.
(42) Wolff, G. A.; Gualtieri, J. G. *Am. Mineral.* **1962**, *47*, 562.
(43) Mishra, R. K.; Thomas, G. *J. Appl. Phys.* **1977**, *48*, 4576.
(44) Waldron, R. D. *Phys. Rev.* **1955**, *99*, 1727.
(45) White, W. B.; DeAngelis, B. A. *Spectrochim. Acta* **1967**, *23A*, 985.
(46) Blyholder, G.; Richardson, E. A. *J. Phys. Chem.* **1962**, *66*, 2597.
(47) Rochester, C. H.; Topham, S. A. *J. Chem. Soc., Faraday Trans. 1* **1979**, *75*(5), 1073.
(48) Sing, K. S. W.; Everett, D. H.; Hawl, R. A. W.; Moscou, L.; Pierotti, R. A.; Rouquerol, J.; Siemienniewska, T. *Pure Appl. Chem.* **1985**, *57*, 609.
(49) Joseph, Y.; Kuhrs, C.; Ranke, W.; Weiss, W. *Chem. Phys. Lett.* **1999**, *314*, 195.
(50) Knozinger, H.; Ratnasamy, P. *Catal. Rev.* **1978**, *17*, 31.
(51) Farmer, V. C. *The infrared spectra of minerals*; Mineralogical Society: London, UK, 1974.
(52) Blyholder, G.; Neff, L. D. *J. Phys. Chem.* **1962**, *66*, 1464.
(53) Chambers, S. A.; Joyce, S. A. *Surf. Sci.* **1999**, *420*, 111.
(54) Ibach, H. *Surf. Sci. Rep.* **1997**, *29*, 193.
(55) Ibach, H. *Surf. Sci. Rep.* **1999**, *35*, 71.
(56) Perriat, P.; Domenichini, B.; Gillot, B. *J. Phys. Chem. Solids* **1996**, *57*, 1641.